ADVANCED MATERIALS
www.advmat.de

2D Ruddlesden–Popper Perovskites for Optoelectronics

*Yani Chen, Yong Sun, Jiajun Peng, Junhui Tang, Kaibo Zheng, and Ziqi Liang**

Conventional 3D organic–inorganic halide perovskites have recently undergone unprecedented rapid development. Yet, their inherent instabilities over moisture, light, and heat remain a crucial challenge prior to the realization of commercialization. By contrast, the emerging 2D Ruddlesden–Popper-type perovskites have recently attracted increasing attention owing to their great environmental stability. However, the research of 2D perovskites is just in their infancy. In comparison to 3D analogues, they are natural quantum wells with a much larger exciton binding energy. Moreover, their inner structural, dielectric, optical, and excitonic properties remain to be largely explored, limiting further applications. This review begins with an introduction to 2D perovskites, along with a detailed comparison to 3D counterparts. Then, a discussion of the organic spacer cation engineering of 2D perovskites is presented. Next, quasi-2D perovskites that fall between 3D and 2D perovskites are reviewed and compared. The unique excitonic properties, electron–phonon coupling, and polarons of 2D perovskites are then be revealed. A range of their (opto)electronic applications is highlighted in each section. Finally, a summary is given, and the strategies toward structural design, growth control, and photophysics studies of 2D perovskites for high-performance electronic devices are rationalized.

1. Introduction

Last several years have witnessed the unprecedented rapid development of a new class of thin-film solar cells based on 3D organic–inorganic halide perovskites. They possess outstanding optical and electronic properties such as strong light harvesting capability, excellent charge transportation, high defect tolerance along with solution processability.[1–7] However, their inherent instabilities over moisture, light, and heat remain crucial hurdles prior to the realization of commercialization.[8,9]

In contrast, the emerging Ruddlesden–Popper 2D perovskites have received increasing attention owing to their superior ambient stability. As shown in **Figure 1**a, the number of publications of 2D perovskites has grown rapidly from 1 in 2014 to 37 in July 2017. The first report of Ruddlesden–Popper phase can be traced back to 1950s when Ruddlesden and Popper discovered three compounds with the K_2NiF_4-type structure, which were Sr_2TiO_4, Ca_2MnO_4, and $SrLaAlO_4$.[10,11] Until recently, however, 2D perovskites have been demonstrated to exhibit abundant and tunable optoelectronic properties, high quantum efficiency, and large specific surface area, which hold good prospect for a range of electronic and optical applications.[12–15] For instance, a respectable power conversion efficiency (PCE) of 12.52% has been achieved for these layered perovskite-based planar solar cells.[16]

The general formula of such 2D perovskite is $(RNH_3)_2A_{n-1}M_nX_{3n+1}$ (n = 1, 2, 3, 4.....), where RNH_3 is a large aliphatic or aromatic alkylammonium spacer cation—for example, 2-phenylethylammonium (PEA) and *n*-butylammonium (*n*-BA), A is monovalent organic cation—typically $CH_3NH_3^+$ (i.e., MA^+) and $HC(NH_2)_2^+$ (i.e., FA^+), M is a divalent metal cation, X is a halide anion, and n represents the number of $[MX_6]^{4-}$ octahedral layers within each quantum well. Figure 1b compares the crystal structures between 3D and 2D perovskites. In 3D perovskites, each layer of $[MX_6]^{4-}$ octahedral is connected with six neighbors at the halogen atoms, forming a network with small organic cations located at the void of the network.[17] By contrast, 2D perovskite crystals can be regarded as n layers of $[MX_6]^{4-}$ octahedral sheets sandwiched by two layers of large organic spacer cations, giving rise to natural multiple-quantum-well structures, in which the inorganic slabs serve as the potential "wells" while the organic layers function as the potential "barriers."[18] The generated excitons are therefore confined within the inorganic slabs (Figure 1c), and when combined with the low dielectric screening from the surrounding organic spacers, much larger exciton binding energy (E_b) are obtained than that of 3D counterparts. Such quantum confinement effect decreases with increasing "well" thickness (n), which can be incrementally tuned by a cautious control of the precursors' stoichiometry. Moreover, different than the hydrophilic MA^+ in 3D $MAPbI_3$ perovskites, the hydrophobic nature of organic spacer and the van der Waals force

Y. Chen, Y. Sun, J. Peng, J. Tang, Prof. Z. Liang
Department of Materials Science
Fudan University
Shanghai 200433, China
E-mail: zqliang@fudan.edu.cn
Dr. K. Zheng
Department of Chemical Physics and NanoLund
Lund University
Box 124 22100, Lund, Sweden
Dr. K. Zheng
Gas Processing Center
College of Engineering
Qatar University
PO Box 2713, Doha, Qatar
The ORCID identification number(s) for the author(s) of this article can be found under https://doi.org/10.1002/adma.201703487.

DOI: 10.1002/adma.201703487

interactions between the adjacent layers impart 2D perovskites with superior air stability.

However, the unique crystal structure of 2D perovskites also brings about some unfavorable characteristics. The insulating organic spacers decrease carrier mobility, cause charge accumulation and radiative recombination losses, and hence significantly undermine device performance. On the other hand, despite that MA^+ cations are free to rotate in each lattice of 3D perovskites, they are to some extent 'frozen' in the 2D structures due to the van der Waals forces and possible π–π interactions in the case of PEA^+. The layer of amine groups is thus positively charged while the neighboring layer of halide anions is negatively charged, resulting in a polar surface between the organic and inorganic layers.[19] Arguably, it is a critical challenge to find effective ways to resolve the above issues. More importantly, the relationship among molecular structure, crystal orientation, transport dynamics and device performance has yet to be established on 2D perovskites, which is detrimental for their further developments of optoelectronics.

In spite of increasing research effort on these 2D Ruddlesden–Popper-type perovskites, there by far exist only one review article which was focused primarily on the spin–orbit coupling effects, band ordering, and quantum confinement of 2D perovskites.[14] In this review, we instead highlight recent advances of 2D perovskites for photovoltaic (PV) and light-emitting diode (LED) applications. First, we will present a detailed discussion of the organic spacer engineering in 2D perovskites and elucidate its crucial role in crystal orientation, transport dynamics, and optoelectronic performance. Second, quasi-2D perovskites, which fall between 2D and 3D perovskites and combine their each merit, will be reviewed and compared. Third, an insight will be offered into unique physical properties of 2D perovskites such as excitonic properties, electron–phonon coupling, and polarons. Finally, we will give a summary and outline the perspectives toward structure, growth, and fundamental photophysics of 2D perovskites for high-performance optoelectronic devices.

Yani Chen graduated with a B.S. in Textile Engineering from Donghua University in 2013. She is currently a Ph.D. candidate in the Department of Materials Science at Fudan University under the supervision of Professor Ziqi Liang. Her research areas focus on perovskite solar cells and organic–inorganic thermoelectrics.

Ziqi Liang obtained his Ph.D. in Polymer Science in the Department of Materials Science and Engineering at Pennsylvania State University in March 2006. He then pursued postdoctoral work at the University of Cambridge from May 2006 to 2008. In June 2008, he joined the National Research Energy Laboratory as a postdoctoral researcher, later to become Scientist III. In September 2012, he joined the Department of Materials Science at Fudan University as a professor. Currently, Prof. Liang's group conducts research on organic and perovskite solar cells, as well as organic and hybrid thermoelectrics.

2. Tailoring Organic Spacer Cation

In comparison to 3D perovskites, one unique advantage of 2D perovskites lies in their facile structure tunability by molecular design of the spacer cations such as alkyl chain length, insertion of π-conjugated segment, and ammonium dications, which in turn greatly impact the optoelectronic properties. **Table 1** lists the molecular structures of organic spacer cation utilized in 2D perovskites.

2.1. $(PEA)_2A_{n-1}M_nX_{3n+1}$

$(PEA)_2(MA)_{n-1}Pb_nX_{3n+1}$ was first synthesized by Nurmikko and co-workers.[18] As shown in **Figure 2**, a series of these compounds can be structurally derived from the 3D $MAPbX_3$

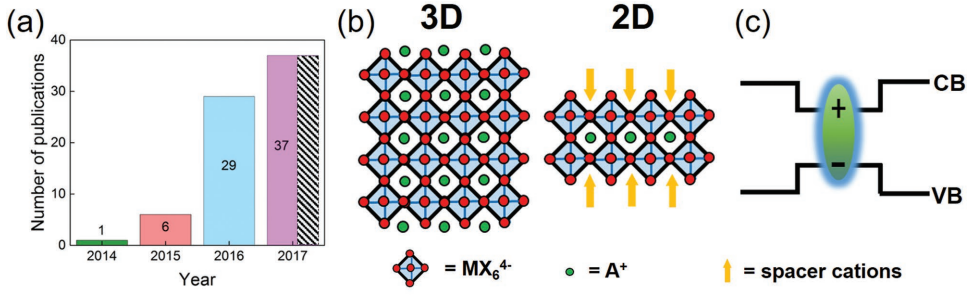

Figure 1. a) The trend in publication numbers of 2D perovskites from 2014 to July 2017 (based on statistic data from Web of Science). b) Schematic of 3D and 2D perovskite structures. c) Characteristic band-alignment in 2D perovskites.

Table 1. Chemical structures of organic spacer cations in 2D perovskites.

Organic spacer cation	Molecular structure
PEA^{+}[18]	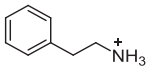
n-BA^{+}[28]	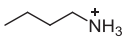
iso-BA^{+}[30]	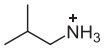
n-$C_6H_{13}NH_3^{+}$[41]	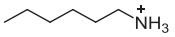
$(FC_2H_4NH_3)^{+}$[44]	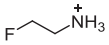
n-$C_8H_{17}NH_3^{+}$[45]	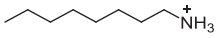
OA^{+}[46]	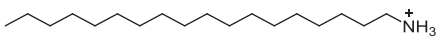
$POEA^{+}$[47]	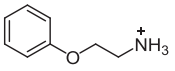
NMA^{+}[48]	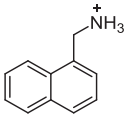
$NAAB^{+}$[50]	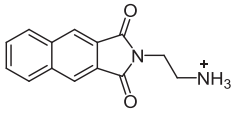
DMEN[51]	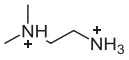
DMAPA[51]	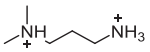
DMABA[51]	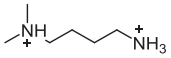
Bd[52]	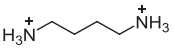
Hd[52]	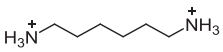
Od[52]	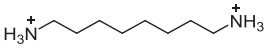
EDBE[53]	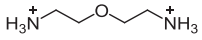
Ava[55]	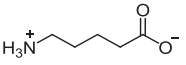

perovskites by slicing along specific crystallographic planes, between which are filled with the PEA cations. The resulting 2D perovskites—for instance, $(PEA)_2PbI_4$—showed weak interaction along the vertical stacking direction as suggested by computationally analyzing the bonding motifs of PEA^{+} with each other and the PbI_4 backbone, respectively.[20]

Decreasing the dimensionality of perovskites will increase both E_g and E_b. Compared to $MAPbI_3$ having $E_g \approx 1.54$ eV and E_b = 13–16 meV,[21] the $(PEA)_2(MA)_{n-1}Pb_nX_{3n+1}$ structures of n = 1 and 2 gave rise to larger E_gs of 2.57 and 2.32 eV as well as exciton absorption bands at 2.35 and 2.15 eV, respectively.[22] Their corresponding E_bs can be estimated from the difference between E_g and exciton absorption energies to be 220 and 170 meV, respectively. Note that the E_b of PEA-based 2D perovskites was found to be dominated by the dielectric confinement, which is distinct from conventional semiconductor quantum wells.[18] The unique quantum and dielectric confinements also impart them with two-photon absorption (TPA) properties. For instance, $(PEA)_2PbI_4$ exhibited a giant TPA coefficient of 211.5 cm MW^{-1}, which was at least one order of magnitude larger than those of 3D perovskite films.[23] In addition, the TPA coefficient was negatively correlated with the thickness of these 2D perovskite flakes, which afforded the potential nonlinear optical applications. Later, a structure–property relationship of phenylalkylammonium cation-based 2D perovskites was revealed by tuning the length of alkyl chains.[19] The density functional theory (DFT) calculations of spin–orbit coupling showed quantum confinement in two- and one-dimensions for the shorter and longer alkyls, respectively. That is, the shortest alkyl chain yielded inorganic sheets of corner-sharing PbI_6-octahedra, while the longer alkyl chain led to structural reorganization, which induced both corner- and face-sharing of the PbI_6-octahedra. As a result, a remarkable blue-shift in photoluminescence (PL) spectra was observed with an increasing length of organic cation.

In 2014, Karunadasa and co-workers demonstrated the first planar solar cell based on 2D perovskites by using $(PEA)_2(MA)_2Pb_3I_{10}$ as optical absorber, yielding a PCE of 4.73% with large V_{OC} = 1.18 V that was attributed to the wide E_g of ≈2.1 eV.[13] Importantly, the $(PEA)_2(MA)_2Pb_3I_{10}$ film showed great stability with little changes on the X-ray diffraction (XRD) patterns and optical absorption spectrum after air exposure of 46 days at a relative humidity (RH) of 52%.

Moreover, the Sargent group demonstrated the good promise of 2D $(PEA)_2(MA)_{n-1}Pb_nX_{3n+1}$ for LED applications. The device showed record-high PL quantum yield (QY) under low excitation fluences. The authors found that the 2D perovskites functioned as charge carrier concentrators to ensure that the radiative recombination successfully outcompeted the carrier trapping and hence nonradiative charge recombination.[15] This overcame the low efficiency of radiative recombination in electroluminescent (EL) devices based on $CH_3NH_3PbI_3$ perovskites. Consequently, LEDs operating at near-infrared wavelengths were produced with an external quantum efficiency (EQE) of 8.8% and a corresponding radiance of 80 W sr^{-1} m^{-2}. In a later report, Jin and co-workers showed a color-pure 410 nm violet-LED, which is rare in both inorganic and organic LEDs, by using layered $(PEA)_2PbBr_4$ as the luminescent material.[24] In this regard, micrometer-sized $(PEA)_2PbBr_4$ nanoplates were grown under solvent vapor annealing, which significantly enhanced the crystallinity and photophysical properties and hence largely increased the EQE of LEDs.

Tin (Sn)-based 2D perovskites have also emerged for high-performance (opto)electronics. In an early attempt, Adachi and co-workers successfully applied $(C_6H_5C_2H_4NH_3)_2SnI_4$ to field-effect transistors (FETs), which exhibited a record hole mobility (μ_h) of 15 cm^2 V^{-1} s^{-1} at room temperature.[25] The high mobility resulted from improved film morphology, increased phase purity, and reduced hole trap density after the treatment of NH_3I self-assembled monolayer. Furthermore, the same

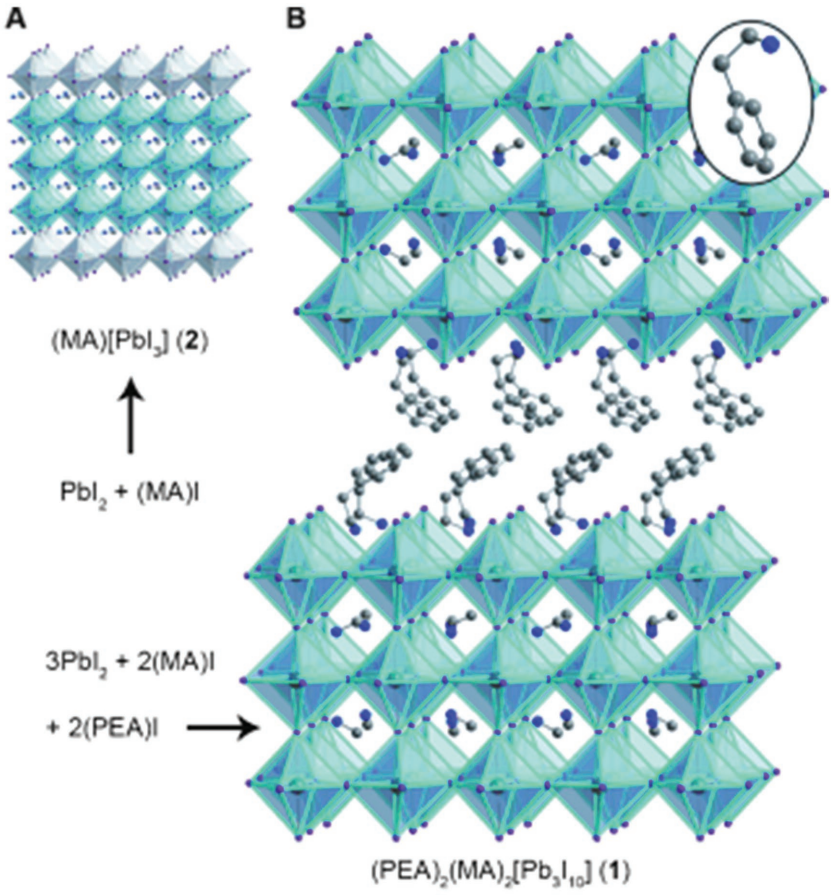

Figure 2. A) Crystal structures of the 3D perovskite $MAPbI_3$ and B) the 2D perovskite $(PEA)_2(MA)_2Pb_3I_{10}$. Inset: a PEA cation in the organic layers. Atom colors: Pb = turquoise; I = purple; N = blue; C = gray. Disordered atoms and hydrogens omitted for clarity. Reproduced with permission.[13] Copyright 2014, Wiley-VCH.

group reported the n-channel transport properties of $PEASnI_4$-based FETs, showing electron mobilities (μ_e) of up to 2.1 $cm^2 V^{-1} s^{-1}$, which was among the highest values in solution-casted perovskites-based FETs.[26] This was realized by employing low-work function Al source/drain electrodes and by inserting a C_{60} layer between the perovskite and the Al electrodes, which assisted to reduce the injection barrier and suppress the electrode degradation.

In another study, 2D Sn-perovskites—$(PEA)_2(FA)_{n-1}Sn_nI_{3n+1}$—was successfully applied in solar cells.[27] At an optimal PEA ratio of 20 mol%, perovskite domains were highly oriented along the perpendicular direction, thereby promoting charge transport. Moreover, $(PEA)_2(FA)_{n-1}Sn_nI_{3n+1}$ possessed high intrinsic thermodynamic stability as indicated from first-principle calculations with respect to the oxidation disproportionation channel. The bulky PEA molecules at the grain boundaries also effectively blocked the oxygen diffusion into the crystal lattice. As a result, $(PEA)_2(FA)_{n-1}Sn_nI_{3n+1}$ based planar solar cells of ITO/NiO_x/$(PEA)_2(FA)_{n-1}Sn_nI_{3n+1}$/[6,6]-phenyl-C61-butyric acid methyl ester (PCBM)/Al yielded a high PCE of 5.94%, which can sustain in air over 100 h without encapsulation.

2.2. $(BA)_2A_{n-1}M_nX_{3n+1}$

In subsequent studies, shorter-chain *n*-butylammonium cation (BA^+)-based 2D lead halide perovskites have been developed. The resulting $(BA)_2(MA)_{n-1}Pb_nX_{3n+1}$ consists of well-defined inorganic $[PbX_6]^{4-}$ layers intercalated with organic BA^+ that act as spacers, thus generating the Ruddlesden–Popper type 2D crystal structures.

Kanatzidis and co-workers reported the first $(BA)_2(MA)_{n-1}Pb_nI_{3n+1}$ perovskite, of which the optical physics and crystal structures were systematically investigated.[28] The optical absorption onset of these compounds displayed sharp edges, suggesting the direct bandgap. It was found that E_g decreased progressively with increasing n values, from 2.24 eV ($n = 1$) to 1.52 eV ($n = \infty$) as shown in **Table 2**. The estimated effective masses of hole and electron carriers are $m_h = 0.14\ m_0$ and $m_e = 0.08\ m_0$, respectively, which were found to be nearly composition independent. When $n \leq 2$, the perovskites exhibited strong PL at room temperature, implying they were suitable for the use of LEDs. For the compounds with $n \geq 3$, they displayed strong light absorption in the visible region, suggesting their good potential for photovoltaic applications. In a following report, small m_h and m_e were obtained in both bulk and monolayer $(BA)_2PbI_4$ by DFT calculation, which can be interpreted by the strong s–p antibonding couplings.[29] With increasing inorganic layer thickness, m_h was found to decrease proportionally, leading to a slightly shifted band edge emission. For example, the absorption band was red-shifted from 502 (single layer) to 519 nm (six layers) and gradually approached 522 nm in bulk $(BA)_2PbI_4$.

As for the crystal structures, all these compounds were crystallized in orthorhombic space groups. In contrast to the centrosymmetric *Pbca* space group adopted in $(BA)_2PbI_4$, the $(BA)_2(MA)Pb_2I_7$, $(BA)_2(MA)_2Pb_3I_{10}$, and $(BA)_2(MA)_3Pb_4I_{13}$

Table 2. Optical parameters of $(BA)_2(MA)_{n-1}Pb_nI_{3n+1}$ perovskites.

Compound	E_g [eV]	Excitonic absorption [eV][a)]	PL [eV]	E_g–PL [meV]	m_e[b)]	m_h[b)]
$(BA)_2PbI_4$	2.43	2.35	2.35	80	0.082	0.144
$(BA)_2(MA)Pb_2I_7$	2.17	2.08	2.12	50	–	–
$(BA)_2(MA)_2Pb_3I_{10}$	2.03	1.96	2.01	20	0.097	0.141
$(BA)_2(MA)_3Pb_4I_{13}$	1.91	1.85	1.90	10	0.094	0.153
$MAPbI_3$	1.50	1.59	1.60	–	–	–

[a)]Position of the excitonic peak in the diffuse reflectance spectra; [b)]Calculated at the DFT–PBEsol level. m_{xz} is reported as the average of the effective mass along the x and z directions and is in units of the bare electron mass. Adapted with permission.[28] Copyright 2016, American Chemical Society.

were crystallized in the polar (*C*2*v*) base-centered *Cc*2*m*, *C*2*cb*, and *Cc*2*m* space groups, respectively. The noncentrosymmetric configurations reflected that the oriented MA cations led to an unquenched net dipole moment within the unit cell. Meanwhile, the inorganic layer thickness can be readily tuned by the molar ratio between the large BA^+ and the small MA^+. Moreover, compared to 3D counterparts, these 2D perovskites showed unique self-assembly ability in thin films, which led to the crystal orientation perpendicular to the substrate and also formed an ultrasmooth surface.

Diverse crystal orientations of perovskites impact differently their optoelectronics performance. There are three types for $(BA)_2(MA)_{n-1}Pb_nI_{3n+1}$ growth on substrate: parallel, perpendicular, and unoriented. "Parallel" means that the extended planes of the $[Pb_nI_{3n+1}]_{(1+n)}^-$ slabs are parallel to the substrate with the remaining layers stacked over them and separated by BA^+ (**Figure 3**a). This type is preferred in FET devices. For "perpendicular," the $[Pb_nI_{3n+1}]_{(1+n)}^-$ slabs are oriented normal to the substrate, which is favorable for charge transport in solar cells. "Nonoriented" suggests that the film has no preferentially oriented growth. In principle, the $n = 1$ compound tends to be parallel with preferential growth along the (110) direction, thus exclusively disclosing the (00l) reflections in XRD patterns (Figure 3b).[12] As n increases, a competition arises between the BA and MA cations, the former of which attempts to confine the perovskite growth within the planar layer while the latter expands the growth outside the layer. For the $n = 2$ compound, the (0k0) reflections are accompanied by the (111) and (202) reflections that reveal the vertical growth relative to the substrate (Figure 3c). Note that the (0k0) reflections for $n = 2$–4 correspond to the (00l) reflection for $n = 1$ and ∞. The $n = 3$ and 4 compounds continue the trend by showing exclusively the (111) and (202) reflections in the absence of (0k0) reflections, clearly indicating the vertical growth of the perovskite compounds (Figure 3d,e).

Taking the above E_g, crystal structure and orientation into account, the compounds of $n = 3$ and 4 are by far the most widely used light-absorbing materials. For example, in the same device structure of fluorine-doped tin oxide (FTO)/TiO_2/$(BA)_2(MA)_{n-1}Pb_nI_{3n+1}$/spiro-OMeTAD/Au, Kanatzidis and coworkers demonstrated the PCEs of 2.39 and 4.02% for the $(BA)_2(MA)_2Pb_3I_{10}$ ($n = 3$) and $(BA)_2(MA)_3Pb_4I_{13}$ ($n = 4$) based solar cells, respectively.[12]

However, the solar cell performance of these above BA-based 2D perovskites was relatively poor due to the inhibited out-of-plane charge transport, which was caused by the insulating spacer cations such as BA^+. To resolve this issue, Mohite and co-workers teamed with Kanatzidis and co-workers applied the hot-casting (HC) technique to fabricate high-quality thin films with preferential cross-plane alignment, which largely improved the PCE from 4.02%[12] up to 12.52%[16] on a regular device structure of FTO/poly(3,4-ethylenedioxythiophene):polystyrene sulfonate (PEDOT:PSS)/$(BA)_2(MA)_3Pb_4I_{13}$/PCBM/Al. Importantly, these devices exhibited much better stability against light and moisture than the 3D counterparts. As indicated in **Figure 4**, the 2D devices remained 60% of their initial efficiency after 2250 h solar light illumination and exhibit greater tolerance under 65% RH than 3D equivalents. The slower degradation could be ascribed to the long and bulky hydrophobic BA group, which can prevent the direct exposure to moisture and thus increase its threshold against degradation.

Nevertheless, when applying such a HC technique, it is difficult to precisely control the substrate temperature during spin-coating, which is undesirable for device reproducibility. To this end, we more recently developed a simple yet effective molecular strategy toward such 2D perovskites by replacing the linear *n*-BA^+ with its isomer—short branched iso-BA^+ (**Figure 5**a).[30] The room-temperature (RT) processed $(iso\text{-}BA)_2(MA)_3Pb_4I_{13}$ showed a remarkable increase of optical absorption and crystallinity in comparison to the $(n\text{-}BA)_2(MA)_3Pb_4I_{13}$ analogue. More importantly, the out-of-plane crystal orientation of $(iso\text{-}BA)_2(MA)_3Pb_4I_{13}$ film was notably enhanced the sharp spots along q_z in grazing-incidence wide-angle X-ray scattering (GIWAXS) images (Figure 5b–e), which dramatically enhanced charge transport and extraction. Consequently, the RT $(iso\text{-}BA)_2(MA)_3Pb_4I_{13}$-based inverted planar solar cell of ITO/C_{60}/$(iso\text{-}BA)_2(MA)_3Pb_4I_{13}$/spiro-OMeTAD/Au yielded a PCE of 8.82%, which is three times higher than that of RT $(n\text{-}BA)_2(MA)_3Pb_4I_{13}$. After applying the HC technique, all these properties were further improved. An impressive PCE of 10.63% was obtained for such 2D perovskite-based planar solar cells. Remarkably, the $(iso\text{-}BA)_2(MA)_3Pb_4I_{13}$ perovskites that were made from both RT and HC methods exhibited superior stability against moisture and oxygen. Among them, the HC sample demonstrated the best ambient stability by maintaining its initial optical absorption after storage of 840 h in an environmental chamber at 20 °C with a RH of 60% without encapsulation.

Recently, Sn-based 2D perovskites have attracted enormous attention because of their more environmental friendliness and lower E_gs varying from 1.83 eV ($n = 1$) to 1.20 eV ($n = \infty$) than the Pb-analogues. However, it is of huge difficulty to fabricate pure Sn-perovskites and their solar cells owing to the facile oxidation of Sn^{2+} to Sn^{4+}. Until most recently, Kanatzidis and co-workers made the first stable working solar cell based on $(BA)_2(MA)_{n-1}Sn_nI_{3n+1}$, which showed a promising PCE of 2.5% for the $n = 4$ member.[31] The device retained more than 90% of their initial performance after 1 month. The reasons are i) the hydrophobic, long BA chains retarded the reaction of perovskite with moisture; ii) the use of triethylphosphine antioxidant in their work suppressed the oxidation of Sn^{2+}. Intriguingly, these 2D perovskites were found very sensitive to the solvent system, which induced crystal alignment. When dimethylsulfoxide (DMSO) solvent was used, 2D perovskites were oriented parallel to the substrate. The orientation was switched to the perpendicular if N,N-dimethylformamide (DMF) was used.

Apart from solar cell applications, photodetectors based on the above BA-based 2D perovskite crystals were successfully fabricated. On customized interdigital graphene electrodes, for instance, both high responsivity of 2100 A W^{-1} and extremely low dark current of 10^{-10} A were achieved.[32] In addition, Huang and co-workers made layered perovskites with different layer numbers, that is, $(BA)_2PbI_4$ ($n = 1$), $(BA)_2(MA)Pb_2I_7$ ($n = 2$), and $(BA)_2(MA)_2Pb_3I_{10}$ ($n = 3$).[33] The corresponding E_gs were 2.33, 2.11, and 2.00 eV, respectively, showing the potential of light detecting for different wavelengths. These photodetectors exhibited highly reproducible ON/OFF switching photoresponsitivity, and the rise/decay times were 28.4/27.5, 8.4/7.5,

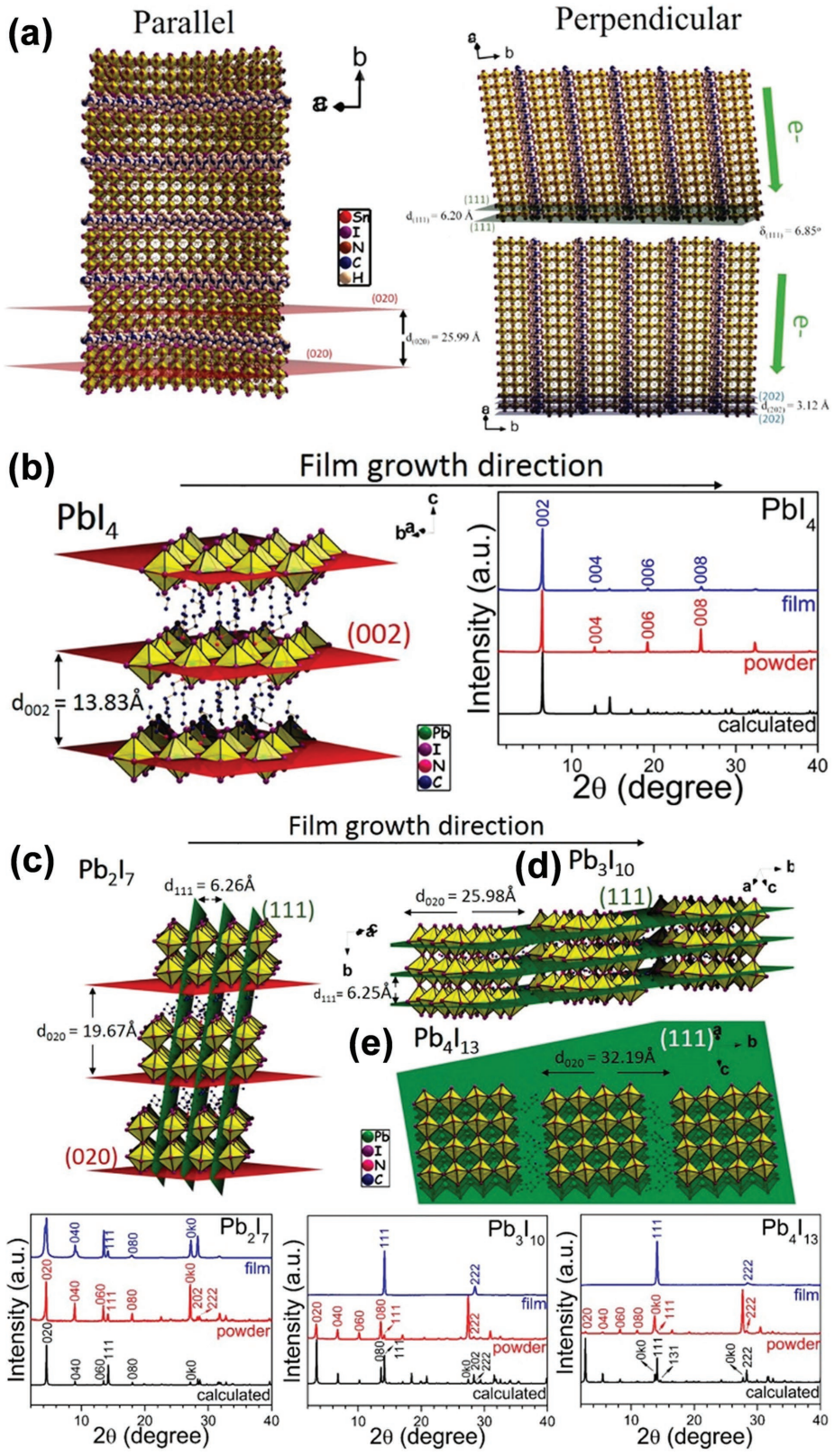

Figure 3. a) Different thin-film growth orientations: (0k0) parallel oriented, (111) almost perpendicular oriented, and (202) perfectly perpendicular oriented. XRD patterns of thin films of b) BA_2PbI_4, c) $(BA)_2(MA)Pb_2I_7$, d) $(BA)_2(MA)_2Pb_3I_{10}$, and e) $(BA)_2(MA)_3Pb_4I_{13}$ perovskites, with the illustration of their respective diffraction planes. a) Reproduced with permission.[31] Copyright 2017, American Chemical Society. b–e) Reproduced with permission.[12] Copyright 2015, American Chemical Society.

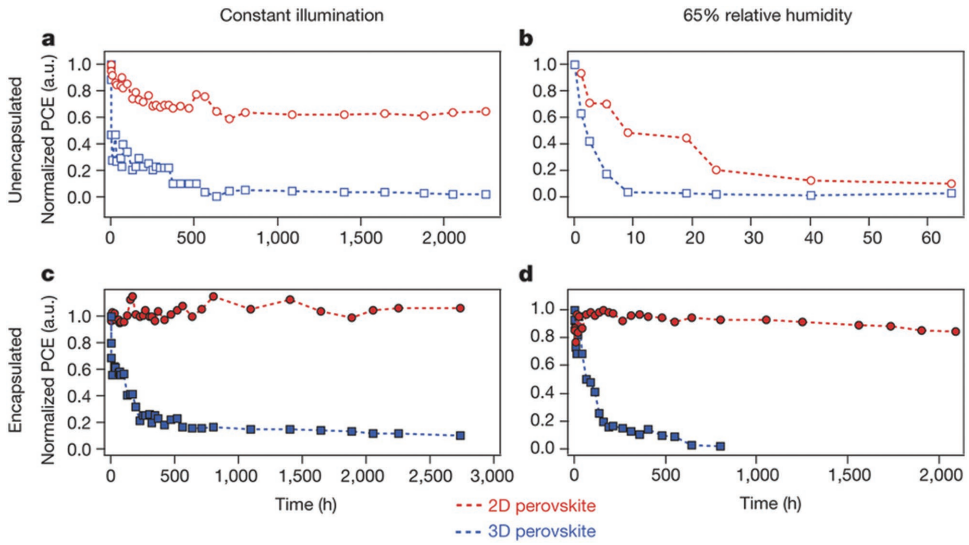

Figure 4. Stability measurements on planar solar cells. Photostability tests under constant AM1.5G illumination for perovskite devices without (a) and with (c) encapsulation. Humidity stability tests under 65% RH in a humidity chamber for perovskite devices without (b) and with (d) encapsulation. Note: red line = 2D $(BA)_2(MA)_3Pb_4I_{13}$, blue line = 3D $MAPbI_3$. Reproduced with permission.[16] Copyright 2016, Nature Publishing Group.

and 10.0/7.5 ms for one-, two- and three-layered perovskites, respectively. The best photodetector performance of three-layered perovskite can be ascribed to its narrower E_g along with better condensed and more compact microstructure than the others. These results revealed the correlation between molecular structures, film microstructures, and photoresponse properties of layered perovskites.

Moreover, the BA-perovskites were found to exhibit strong luminescence. For instance, Yang and co-workers developed the solution-phase growth of single-crystalline $(BA)_2PbBr_4$ 2D sheets, which exhibited strong purple-blue PL spectrum.[34] As shown in **Figure 6**a, these sheets were uniform and square with a thickness of 1.6 ± 0.2 nm as quantified by atomic force microscopy (AFM) height image. Figure 6b, c show transmission electron microscopy (TEM) image of and selected-area electron diffraction (SAED) pattern, respectively. The calculated average in-plane lattice constants were a = 8.41 Å and b = 8.60 Å, which were slightly larger than those in the bulk crystal (a = 8.22 Å and b = 8.33 Å). Such unusual lattice expansion led to a shift of E_g relative to the bulk crystal. Furthermore, the E_g can be regulated by varying the inorganic layer thickness and compositions. As an another example, the tetrahedral molecular ion (BF_4^-) was inserted into the 2D perovskites.[35] The as-synthesized $(BA)_2Pb(BF_4)_4$ showed optical absorption in UV region.

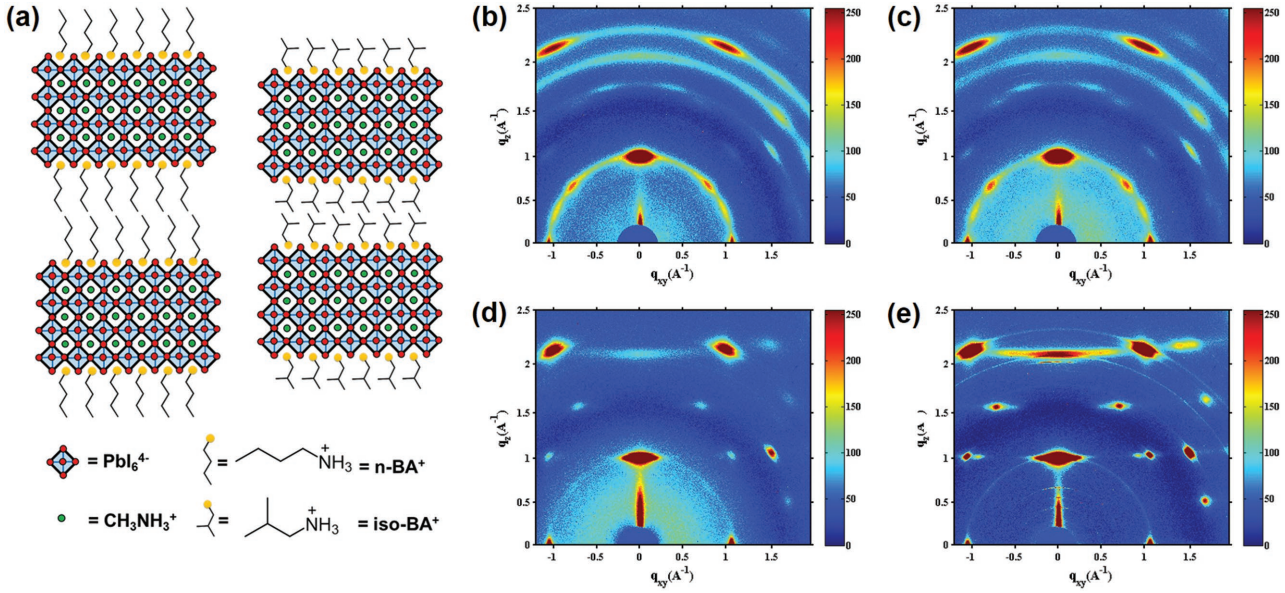

Figure 5. a) Schematic crystal structures of the $(n\text{-}BA)_2(MA)_3Pb_4I_{13}$ and $(iso\text{-}BA)_2(MA)_3Pb_4I_{13}$ perovskites. GIWAXS images of b) RT and c) HC $(n\text{-}BA)_2(MA)_3Pb_4I_{13}$, d) RT, and e) HC $(iso\text{-}BA)_2(MA)_3Pb_4I_{13}$ perovskites. Reproduced with permission.[30] Copyright 2017, Wiley-VCH.

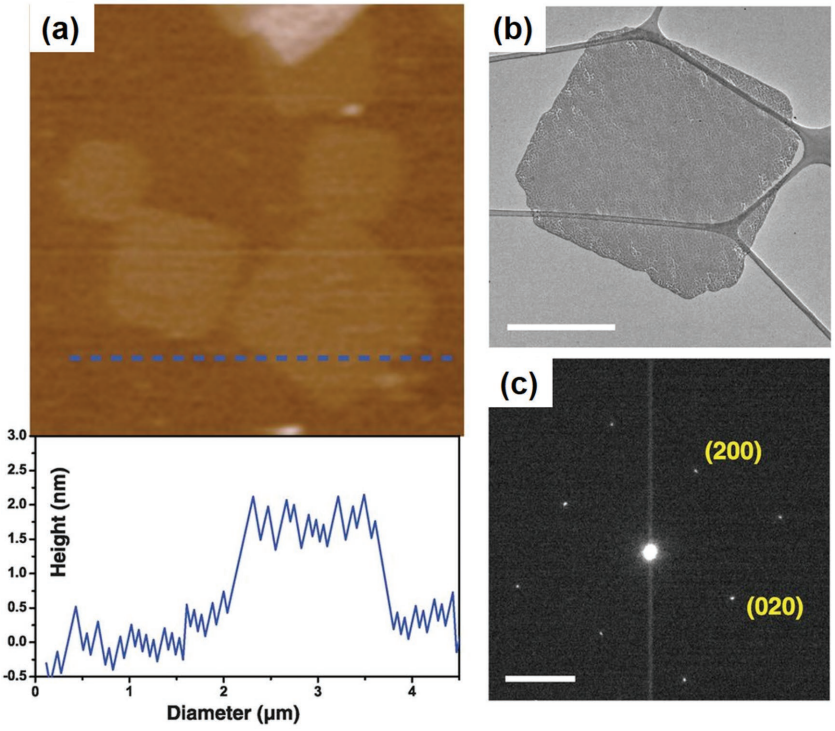

Figure 6. a) AFM image and height profile of several $(BA)_2PbBr_4$ single layers. b) TEM image of a thin $(BA)_2PbBr_4$ sheet. Scale bar is 1 mm. c) Electron diffraction pattern of a thin sheet of $(BA)_2PbBr_4$. Scale bar is 2 nm^{-1}. Reproduced with permission.[34] Copyright 2015, American Association for the Advancement of Science.

Further incorporation of Br^- and I^- anions rendered strong blue and green luminescence, respectively.

The unique multiple quantum well (MQW) structures of 2D perovskites are believed to offer a viable avenue to high-performance LEDs. For instance, deep saturated red emission was obtained for $(BA)_2(MA)_2Pb_3I_{10}$ with a peak EQE of 2.29% and a maximum luminance of 214 cd m^{-2}.[36] Green and blue LEDs were also fabricated by Br and Br/Cl substitutions. Likewise, an addition of long-chain BAX (X = I, Br) to the 3D perovskite precursor solution suppressed the crystal growth, which produced the crystallites as small as 10 nm and significantly reduced the film roughness down to 1 nm.[37] These BAX-included perovskites displayed enhanced yet blue-shifted PL and EL than 3D counterparts. These perovskites based LEDs gave rise to high EQEs of 10.4% for the I-system and 9.3% for the Br-system with significantly improved the shelf and operational stability.

Interestingly, 2D perovskites can also serve as ligands of inorganic semiconductor quantum dots (QDs). For instance, Sargent and co-workers passivated the surface of PbSe quantum dots by a new perovskite ligand exchange, where ammonium/amine was in situ substituted by butylamine.[38] This enabled the interdigitation of $(BA)_2PbI_4$ among PbSe nanostructures. The average spacing between two adjacent PbSe nanowires was close to the thickness of single atomic layer of $(BA)_2PbI_4$ perovskite, indicating the formation of a new self-assembled perovskite heterocrystal hybrid. In addition, BA^+ was successfully incorporated into all-inorganic $CsPbI_3$ to form 2D $BA_2CsPb_2I_7$ perovskite.[39] It exhibited the preferentially oriented growth perpendicular to the substrate, which favored charge separation and transport in solar cells. Moreover, $BA_2CsPb_2I_7$ can stabilize the black phase of $CsPbI_3$. A PCE of 4.84% was thus achieved in the device of FTO/TiO_2/$BA_2CsPb_2I_7$/spiro-OMeTAD/Au. The device maintained 92% of its initial PCE after aging under ambient conditions for 30 d without capsulation.

The electronic properties of single-layer 2D hybrid perovskites BA_2MI_4 (M = Ge, Sn, and Pb) were also investigated by means of DFT at the Heyd–Scuseria–Ernzerhof (HSE06) hybrid functional level.[40] The calculated E_gs of atomically thin BA_2GeI_4 and BA_2SnI_4 were 1.74 and 1.45 eV, respectively, which are potential candidates as lead-free 2D perovskites for numerous applications. For instance, the strong exciton effects in BA_2MI_4 were beneficial for PL and contributed to photocurrent in solar cells when contacting with appropriate transporting layers. Further improved optoelectronic performance may be attained by heterogeneously stacking of 2D perovskite with other layered materials.

2.3. Other Types

In addition, the modifications of PEA^+ and BA^+, and the emerging dications have been successfully developed to enhance the hydrophobilicty, improve charge separation, and increase the quantum efficiency of 2D perovskites and their devices.

2.3.1. BA Modification

Novel spacers have been recently developed based on BA^+ modification. For example, n-$C_6H_{13}NH_3^+$, which has a longer alkyl chain than BA^+, was incorporated into MA, FA, and Cs-based perovskites, respectively.[41] Among them, $(n\text{-}C_6H_{13}NH_3)_2FAPb_2I_7$ exhibited partly perpendicular crystal growth relative to the substrate, which facilitated charge transport in solar cells and hence achieved a PCE of 1.03%. Further improvements of photovoltaic properties are anticipated by optimized material or device architectural design. The same cation based non-lead 2D perovskites, $(C_6H_{13}NH_3)_2MCl_4$ (M = Cu^{2+}, Mn^{2+}, Cd^{2+}), were also made.[42] They underwent reversible solid–solid phase transitions by changing the solvent medium in which they were immersed. Moreover, the transition temperature shifted to room temperature for the Cu^{2+} and Cd^{2+} based compounds. This was owing to the reduced effective pressure through the interactions between the solvent and the perovskite surface.

Later, Banerjee and co-workers systematically examined the role of the chain length and the concentration of alkylammonium ions ($C_nH_{2n+1}NH_3^+$, n = 4, 6, 8, 12, and 18) on the crystal growth of perovskites.[43] Alkylammonium ions were strongly electrostatically bound to the faces of the perovskite crystals, thus restricting the crystal growth along the vertical direction. It

was further found that the longer chain and the higher concentrations led to a reduction of layer thickness. Tunable thickness that spans between one and six-unit cells were obtained, corresponding to the emissive range of 430–520 nm.

In order to further improve moisture-resistance of 2D perovskites, 2-fluoroethylammonium cation, $(FC_2H_4NH_3)^+$, was chosen as an alternative organic spacer.[44] Two phase transitions took place in $(FC_2H_4NH_3)_2PbCl_4$ when increasing temperature. The first one occurred at 87 °C caused by structural changes in the heavy lattice while the second at 107 °C was likely related to orientational changes in the organic sublattice. DFT calculations tracked the origin of such observed distortion of the $PbCl_6$ octahedra in $(FC_2H_4NH_3)_2PbCl_4$ to the formation of hydrogen bonds between the inorganic and organic sublattices. On the other hand, $(FC_2H_4NH_3)_2PbCl_4$ had an indirect E_g of 3.27 eV. Upon excitations below E_g, a strong and broad PL spectrum was observed, which can be assigned to the exciton self-trapping due to a strong coupling of the excited states to the lattice distortions. Additionally, the addition of F atom induced a large dipole moment within the layered structure, which might lead to an increased polarity of the lattice and thus improved charge separation and carrier lifetime. Surprisingly, $(FC_2H_4NH_3)_2PbCl_4$ preserved its integrity upon exposure to ambient atmosphere for several months.

Nanoplatelets in the form $L_2[ABX_3]_{n-1}BX_4$ were newly synthesized where L is an organic ligand (e.g., octylammonium, BA).[45] The n, B, and X had a strong influence on the absorption and emission energy, while A cation significantly affected the nanoplatelet stability and PLQY. By halide substitution, continuous spectral tunability can be obtained over the spectral range from 2.2 to 3.7 eV. Moreover, the ligand length played a critical role in the periodicity of nanoplateletes, which had relatively large lateral dimensions of 100 nm–1 μm.

Octadecylamine (OA), a frequently used capping ligand in quantum dots, has also been incorporated in 2D perovskites. For instance, $(OA)_2FA_{n-1}Pb_nBr_{3n+1}$ microplatelet film was made and used for photodetectors.[46] Upon its immersion in FA^+ solution, an ion exchange reaction between OA^+ and FA^+ occurred, which increased the dimensionality of 2D perovskites. This hence alleviated the quantum confinement effect and facilitated the separation of bound electrons and holes. In addition, the starting discrete microplatelets were fused, thus circumventing undesired interfacial scattering while promoting interdomain charge transport. Therefore, the immersed $(OA)_2FA_{n-1}Pb_nBr_{3n+1}$ based photodetectors showed an increase of EQE and responsivity up to 7100% and 32 A W^{-1}, respectively.

2.3.2. PEA Modification

Likewise, various structures based on PEA^+ spacers have recently emerged. One such example is 2-phenoxyethylamine (POEA), which has an extra oxygen atom in the widely used PEA chain of 2D perovskites.[47] On the one hand, the amine head groups were linked to the perovskite surface by substituting partial $CH_3NH_3^+$. On the other hand, the benzene end groups of POEA interacted through π–π stacking and led to the formation of layered perovskite structure upon a certain amount of molecule loading. The transition from $CH_3NH_3PbBr_3$ 3D bulk film to layered structure induced a hypsochromic shift of emission from green to blue. The optimized LED devices reached a maximum EQE of 2.82% and a high current efficiency (CE) of 8.23 cd A^{-1}.

Wang et al. introduced 1-naphthylmethylamine iodide (NMAI) in the precursor solution of $FAPbI_3$, which produced self-organized MQWs with good film morphologies.[48] The absorption spectrum of generated 2D perovskites showed multiple shoulder bands, indicating a mixture of compounds with different exciton energies. Thus, a cascade energy structure of 2D perovskites can be formed for the use in LED devices. The regions of lower E_g were effectively confined by those with higher E_gs, resulting in highly efficient radiative decay. Unexpectedly, the large interfacial areas between different E_g regions did not cause luminescence quenching. Consequently, these MQW-based LEDs exhibited a record EQE of 11.7% with good stability and an exceptionally high energy conversion efficiency of 5.5% at a current density of 100 mA cm^{-2}. Later, the same group employed the same spacer cations in Cs-perovskites.[49] The formation of cubic phase can be realized at low temperature owing to the MQW structure. The inclusion of chloride further improved the crystallization and optical properties of Cs based MQWs, leading to a low turn-on voltage of 2.0 V, a maximum EQE of 3.7% and a peak luminance of 440 cd m^{-2} at 4.0 V in LEDs.

An organic luminophore, 2,3-naphthalimide-ethylammonium molecule (NAAB), was also incorporated into lead bromide type perovskites and generated the 2D structure.[50] A substantial increase of the brilliance and luminescence efficiency in LEDs was thus acquired.

2.3.3. Dications

Aside from monoammonium, the inclusion of dications has proved as an effective strategy to create 2D layered structures. Kanatzidis and co-workers designed three new 2D lead bromide perovskite compounds by using a series of bifunctional ammonium dications.[51] As shown in Table 1, α-(DMEN)$PbBr_4$ where DMEN = 2-(dimethylamino)ethylamine adopted a unique corrugated layered structure in space group Pbca with unit cell a = 18.901(4) Å, b = 11.782(2) Å, and c = 23.680(5) Å; (DMAPA)$PbBr_4$ where DMAPA = 3-(dimethylamino)-1-propylamine) crystallized in P21/c with a = 10.717(2) Å, b = 11.735(2) Å, c = 12.127(2) Å, and β = 111.53(3)°; (DMABA)$PbBr_4$ where DMABA = 4-dimethylaminobutylamine) adopted Aba2 with a = 41.685(8) Å, b = 23.962(5) Å, and c = 12.000(2) Å. The organic cations had a huge influence on the templating of the inorganic layers and the resulting optical properties. The larger the octahedral distortion of $[PbBr_6]^{4-}$ slabs became, the broader PL emission and the longer lifetime were attained. Among these three compounds, α-(DMEN)$PbBr_4$, which was stabilized by "chelating effect" of hydrogen bonding interactions, exhibited the most distorted structure. As a consequence, it showed white-light emission with a color rendering index (CRI) of 73 that is comparable to a fluorescent light source. The white-light emission originated mainly from the role of self-trapped excitons.

Table 3. Summary of 2D perovskite structures and their solar cell performance.

Structure	E_g [eV]	Device configuration	Jsc [mA cm^{-2}]	V_{oc} [V]	FF	PCE [%]
$(PEA)_2(MA)_2Pb_3I_{10}$	2.1	FTO/c-TiO_2/ perovskite/spiro-OMeTAD/Au	6.72	1.18	0.60	4.73[13]
$(PEA)_2(FA)_8Sn_9I_{28}$	N/A	ITO/NiO_x/perovskite/PCBM/Al	14.44	0.59	0.69	5.94[27]
$(BA)_2(MA)_2Pb_3I_{10}$	1.85	FTO/m-TiO_2/perovskite/spiro-OMeTAD/Au	9.42	0.93	0.46	4.02[12]
$(BA)_2(MA)_3Pb_4I_{13}$	1.60	FTO/m-TiO_2/perovskite/spiro-OMeTAD/Au	9.09	0.87	0.30	2.39[12]
$(BA)_2(MA)_3Pb_4I_{13}$ (HC)	N/A	FTO/PEDOT:PSS/perovskite/PCBM/Al	16.76	1.01	0.74	12.51[16]
(iso-BA)$_2(MA)_3Pb_4I_{13}$ (RT)	1.78	ITO/C_{60}/perovskite/spiro-OMeTAD/Au	14.87	1.14	0.52	8.82[27]
(iso-BA)$_2(MA)_3Pb_4I_{13}$ (HC)	1.74	ITO/C_{60}/perovskite/spiro-OMeTAD/Au	16.54	1.20	0.53	10.63[30]
$(BA)_2(MA)_3Sn_4I_{13}$	1.42	FTO/m-TiO_2/perovskite/PTAA:TPFB/Au	24.1	0.23	0.46	2.53[31]
$(BA)_2(MA)_3Pb_3SnI_{13}$	2.01	ITO/PEDOT:PSS/perovskite/PCBM/Bphen/Al	8.97	0.68	0.59	3.57
$BA_2CsPb_2I_7$	2.2	FTO/c-TiO_2/perovskite/spiro-OMeTAD/Au	8.88	0.96	0.57	4.84[39]
$(n\text{-}C_6H_{13}NH_3)_2FAPb_2I_7$	N/A	FTO/c-TiO_2/perovskite/spiro-OMeTAD/Au	2.86	0.64	0.55	1.03[41]
$[NH_3(CH_2)_4NH_3]PbI_4$	2.37	FTO/m-TiO_2/perovskite/spiro-OMeTAD/Ag	2.89	0.87	0.43	1.08[52]

Note that J_{sc}, short-circuit current; V_{oc}, open-circuit voltage; FF, fill factor.

As such, the Gardner group recently synthesized three types of 2D perovskites based on diammonium with varying alkyl chain lengths—$[NH_3(CH_2)_4NH_3]PbI_4$ ($BdAPbI_4$), $[NH_3(CH_2)_6NH_3]PbI_4$ ($HdAPbI_4$), and $[NH_3(CH_2)_8NH_3]PbI_4$ ($OdAPbI_4$).[52] The incorporated diammonium cations acted to bridge the neighboring PbI_4^- planes. As the chain length was increased, the E_gs became larger, giving 2.37, 2.44, and 2.55 eV for $BdAPbI_4$, $HdAPbI_4$, and $OdAPbI_4$, respectively. Both $BdAPbI_4$ and $HdAPbI_4$ presented impressive thermal stability in excess of 200 °C. Solar cells based on $BdAPbI_4$ delivered a PCE of 1.08%. Similarly, the Jen and co-workers employed alkyl diammonium iodide to passivate crystallographic defects of $CH_3NH_3PbI_3$ film on the film surface and at the grain boundaries while forming the 2D perovskite structures.[53] The molecular structure of the diammonium iodide was found to affect strongly the surface morphology and phase purity of perovskite. Both $NH_3I(CH_2)_4NH_3I$ and $NH_3I(CH_2)_2O(CH_2)_2NH_3I$ (EDBE) induced the 3D-to-2D perovskite phase transformation, while $NH_3I(CH_2)_8NH_3I$ with a longer alky chain failed to form 2D structure because of the elevated activation energy. However, in their work, the formation of layered structure was unfavorable for charge transport in device due to the insulating nature of organic spacers. In another work, 2D $(EDBE)PbCl_4$ perovskite crystals were manifested as promising X-ray scintillator materials owing to their low intrinsic trap density, nanosecond fast response, and potentially high light yield.[54] In particular, their large E_b helped reduce the strong thermal quenching effects in 3D analogues. Thus, a moderate light yield of 9000 photons per MeV was achieved even at room temperature.

Recently, Zhao and co-workers developed crosslinked $NH_3C_4H_9COO(CH_3NH_3)_nPb_nBr_{3n}$ perovskites by addition of a bifunctional 5-aminovaleric acid, $NH_2C_4H_9COOH$ (AVa), into $MAPbBr_3$ precursor solutions.[55] The NH_3^+ and COO^- end groups were anticipated to occupy the MA^+ positions and Br^- sites of the neighboring two $MAPbBr_3$ unit cells, respectively. By changing the AVa/MA ratio, the quantum confinement induced optical properties of $AVa(CH_3NH_3PbBr_3)_n$ varied gradually. As a result, a PLQY of up to 80% was obtained for $Ava(MAPbBr_3)_2$.

2.4. Summary

Tables 3 and **4** summarize all the above 2D perovskites based solar cell and LED performance, respectively. On the one hand, it can be seen that the PCEs in solar cells are notably lower as compared to that of 3D counterparts (Table 3). The decreased performance mainly lies in the Jsc loss, which is attributed to inefficient exciton dissociation and unfavorable charge recombination. To resolve it, the hot-cast method of fabricating 2D perovsktie thin films has proved as an effective means to improve crystal orientation and facilitate charge transport. On the other hand, for the LED applications, 2D perovskites with larger n outperformed those with smaller n. This may be correlated with electrical conductivity in thin film and carrier transportation in device. Therefore, it is difficult for electrons and holes to inject into the emitting layer when n is too small. In contrast, when n becomes larger, it is always a mixture of self-organized 2D perovskites with different E_g s and 3D analogue, thereby forming cascade-energy-level alignment and promoting radiative decay.

3. Quasi-2D Perovskites

Besides tailoring the functional spacer cations, 2D perovskites present greater room of modulating properties than their 3D counterparts by varying n. As above mentioned, in 2D perovskites with $n \leq 4$ series, E_gs are still large for solar cell applications. One may tempt to wonder what if $n > 4$? As n further increases, E_gs decreases and the properties will approach those of 3D counterparts, thus forming quasi-2D structures. These quasi-2D materials are promising candidates for use in those optoelectronic applications that simultaneously require good stability and high efficiency.

Table 4. Summary of 2D perovskite structures and their OLED performance.

Structure	Device configuration	Peak PL/EL [nm]	PLQY/PLQE [%]	CE [cd A^{-1}]	PE [lm W^{-1}]	V_{ON} [V]	Lumin [cd m^{-2}]	EQE [%]
$(PEA)_2(MA)_4Pb_5I_{16}$	ITO/TiO_2/perovskite /F8/MoO_3/Au	760 (EL)	10.6 (PLQY)	N/A	N/A	3.8	N/A	8.8[15]
$(PEA)_2PbBr_4$	ITO/PEDOT:PSS /perovskite/TPBi/Ca/Al	407/410	N/A	N/A	N/A	2.5	N/A	0.038[24]
$(BA)_2(MA)_2Pb_3I_{10}$	ITO/PEDOT:PSS/polyTPD/perovskite/TPBi/LiF/Al	700 (EL)	N/A	0.1	N/A	2.7	214	2.29[36]
BAI:$MAPbI_3$ = 1:5	ITO/polyTPD/perovskite/TPBi/LiF/Al	750/748	1.9 (PLQY)	0.09	0.10	N/A	N/A	10.4[37]
BABr:$MAPbBr_3$ = 1:5	ITO/perovskite/TPBi/LiF/Al	516/513	7.0 (PLQY)	17.1	13.0	N/A	N/A	9.3[37]
$MAPbBr_3$ with 30% POEA	ITO/PEDOT:PSS/perovskite/TPBI/Ba/Al	520/520	N/A	8.23	N/A	N/A	64.20	2.82[47]
$(NMA)_2FAPb_2I_7$	ITO/ZnO/perovskite/TFB/MoOx/Au	763 (EL)	67 (PLQE)	5.5	N/A	1.3	N/A	11.7[48]
$NCPI_6Cl$	ITO/ZnO/perovskite/TFB/MoOx/Au	688 (EL)	20 (PLQE)	N/A	N/A	2.0	440	3.7[49]

Note that PE, power efficiency; V_{TO}, Turn-on voltage; Lumin, Luminance. $NFPI_7$ is the mixture of $(NMA)_2FA_{n-1}PbnI_{3n+1}$ with different n values and $NCPI_6Cl$ represents a mixture of $(NMA)_2PbI_4$ and $(NMA)_2(CsPbI_2Cl)PbI_4$.

For instance, Etgar and co-workers utilized quasi-2D perovskites of $(PEA)_2(MA)_{n-1}Pb_nBr_{3n+1}$ (n = 40, 50, 60) in solar cells of FTO/TiO_2/$(PEA)_2(MA)_{n-1}Pb_nBr_{3n+1}$/(spiro-OMeTAD)/Au.[56] The formation of the 2D perovskite structure was indicated by the low angle reflections about 5.3° in the XRD patterns. A high V_{OC} of 1.3 V or 1.46 V was obtained when using hole-transporting layer or without it, respectively, which showed corresponding PCEs of 6.3% and 8.5%, among the highest reported values. Such high V_{OC} may result from the lower carrier mobility in quasi-2D perovskites, which was further supported by both ab initio calculations and charge extraction measurements. In this aspect, fewer charge carriers were accumulated at the selective contacts, resulting in better charge extraction and less carrier recombination. Moreover, the DFT simulations suggested an increase of electrical conductivity as n became larger, in agreement wth good device performance.

Later, Lee and co-workers developed such quasi-2D perovskites that mixed $(PEA)_2PbBr_4$ with $MAPbBr_3$, which led to high-efficiency green LEDs.[57] Note that in this respect, it is difficult to determine the n value. The optimal device with a MA:PEA ratio = 16 showed the highest current efficiency of 4.90 cd A^{-1} and the maximum luminance of 2935 cd m^{-2}, respectively, which are much higher than those of LEDs that used pure 3D or 2D perovskite materials. The reasons are a combination of improved film quality, enhanced exciton confinement and reduced trap density.

However, if n becomes too large, the formation of 2D perovskite domains will disappear, thus generating quasi-3D perovskites. For example, Jen and co-workers fabricated mixed-cation $FA_xPEA_{1-x}PbI_3$ perovskites by changing the molar ratios (N) of FAI to PEAI.[58] The larger PEA cation was assembled on both lattice surface and grain boundaries to form quais-3D perovskite structures and served as molecular locks to tighten $FAPbI_3$ domains. Thus, the transition energy from the black phase to yellow phase was raised, resulting in improved phase stability. In addition, the optical absorbance of $FA_xPEA_{1-x}PbI_3$ films with N of 20–60 was increased in comparison to that of the pristine $FAPbI_3$ ($N = \infty$), indicating that PEA^+ can aid to enhance the crystallinity. The corresponding E_g only showed a slight increase from 1.518 to 1.524 eV when N was increased from 10 to infinity. Moreover, as N increased, the corresponding full width at half maximum (FWHM) was gradually decreased, indicative of smaller crystal sizes and decreased vacancies or dislocation in perovskite film. Consequently, the N = 40 compound based solar cells of ITO/NiO_x/$FA_xPEA_{1-x}PbI_3$/PCBM/C_{60}/Ag afforded a very high PCE of 17.7%.

Nonetheless, in all these quasi-2D perovskites, a trade-off existed between decreasing electrical conductivity and improving ambient stability. It is however challenging to solve this issue because of the intrinsic low carrier mobility of 2D perovskites. We propose that it could be resolved by modulation of n or incorporating smaller spacer cations yet with higher charge carrier mobility, while maintaining 2D perovskite structures.

On the other hand, the construction of 2D/3D heterojunction in perovskite solar cells was manifested as an effective way to enhance both device performance and moisture stability.[59,60] For instance, an addition of $(PEA)_2(MA)_4Pb_5I_{16}$ 2D thin layer on the top of $MAPbI_3$ caused a reorganization and reorientation of the $MAPbI_3$ layer, leading to reduced recombination loss within the device.[59] One most recent work built up 2D/3D $(HOOC(CH_2)_4NH_3)_2PbI_4/CH_3NH_3PbI_3$ junction based solar cells with a large area of 10 × 10 cm^2, which exhibited outstanding air-stability by maintaining a PCE of 11.2% over 10 000 h (i.e, one year) with zero loss under standard ambient conditions.[60]

4. Charge Carrier Dynamics

4.1. Excitonic Nature

Excitons are formed with a high E_b (0.1–0.5 eV) in 2D perovskites because dielectric screening is low from the surrounding organic ligands and electrons and holes are confined within the 2D inorganic lattices.[61,62] The transient photoconductivity experiments by time-resolved terahertz (THz) spectroscopies verified that charge conduction occurred predominantly along the 2D lead iodide planes, which further verified the asymmetric confinement of 2D perovskites.[63] As the inorganic layer thickness decreases, the quantum confinement in the direction perpendicular to the plane leads to a widening of E_g. Consequently, the pronounced exciton absorption and emission peaks can be observed, which blue-shifted as n decreased as shown

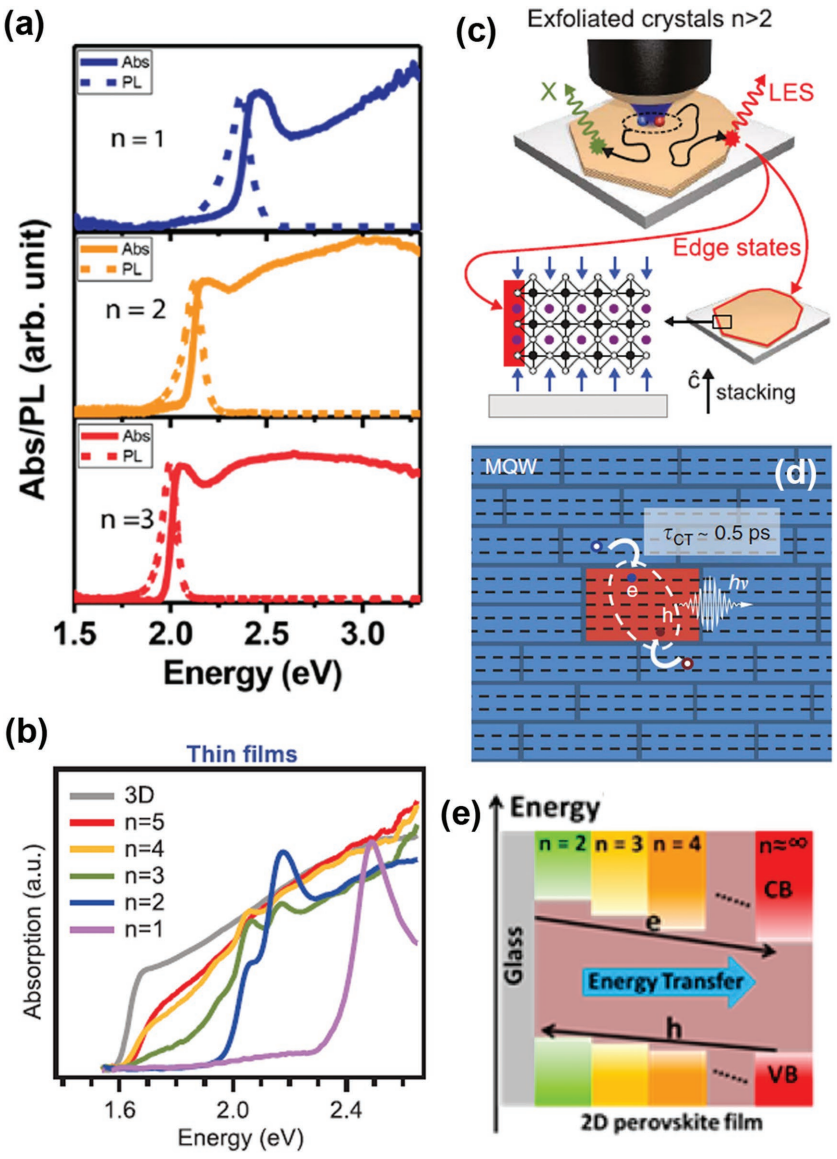

Figure 7. Absorption and PL spectra of 2D perovskite a) monophase structures and b) hybrid phase films. c) Schematic of the absorption and PL processes in 2D perovskite exfoliated crystals with $n > 2$. d) Illustration of charge injection, exciton localization, and subsequent carrier recombination from the thin quantum wells to the self-assembled thick quantum wells dopants in 2D perovskites. e) Three possible carrier transfer mechanisms, electron and energy transfers from small-n to large-n perovskites, and hole transfer from large-n to small-n perovskites, are all energetically allowed. a) Reproduced with permission.[61] Copyright 2016, American Chemical Society. b,c) Adapted with permission.[64] Copyright 2017, American Association for the Advancement of Science. d) Reproduced with permission.[62] Copyright 2017, Nature Publishing Group. e) Reproduced with permission.[65] Copyright 2017, American Chemical Society.

in **Figure 7**a.[61] However, solution-processed 2D perovskites always comprise hybrid perovskite phases with different n values, whereas the molar ratio of precursors is intended for a single phase as indicated by multiple exciton response peaks in absorption spectra, which are shown in Figure 7b.[64]

Given the structural inhomogeneity in 2D perovskites, the charge carrier dynamics is much more complicated when compared with their 3D counterparts. One of the most unique phenomena is the spatial redistribution of the photogenerated species observed by numerous research groups. Regardless of the sample variation, different interpretations have been provided by far. For instance, Blancon et al. unveiled the existence of "edge states" at the interface of the perovskite layers when $n > 2$ observed by PL microscopy.[64] These states provided a direct pathway for dissociating excitons into longer-lived free carriers as shown in Figure 7c. Such dissociated free carriers are expected to be protected from nonradiative decay mechanisms such as electron–phonon coupling or electronic impurities and then greatly contribute to photocurrent in solar cells or radiative recombination for EL.

Another observation is the efficient charge transfer from thin 2D layer phase (i.e., small n) to the adjacent thick layer phase (i.e., large n) as suggested in Figure 7d.[62] Such charge transfer process was extremely efficient (≈0.5 ps) that could suppress most of the carrier recombination pathway and led to the exciton localization at those thick quantum wells ($n > 5$). The excitonic recombination in those thick multiquantum-wells should take place at much higher decay rate and efficiency than bimolecular recombination in 3D perovskites for efficient EL.

However, in thick 2D perovskite films, the timescale of internal charge transfer is dominated by the geometries of the perovskites where the mixture phases are largely separated.[62] In this scenario, internal charge diffusion observed in thick 2D films is within hundreds of ps timescale. In addition, a systematical photophysical study on typical $(BA)_2(MA)_{n-1}Pb_nI_{3n+1}$ 2D perovskite film by using transient PL and absorption spectroscopies implied that the small-n phases should primarily locate at the bottom surface while the large-n phase reside at the upper surface of the film.[65] In this regard, electron and hole transfers occurred in the opposite direction according to the energy alignment as shown in Figure 7e. This internal charge separation can accumulate both electron and hole carriers on the spatially separated upper and bottom surfaces of perovskite film.

In addition to singlet excitons, efficient generation of triplet excitons was also revealed in $(CH_3NH_3)_2Pb(SCN)_2I_2$ 2D perovskites.[66] This was evidenced by the energy discrepancy between absorption and emission transition from steady-state spectroscopies as well as triplet–triplet energy transfer from $(CH_3NH_3)_2Pb(SCN)_2I_2$ to a variety of attached low-energy triplet chromophores. The resulting phosphorescence of triplet excitons was >47 times more intense than its bandgap fluorescence, with an enhanced PLQE at low

temperature due to the structural transition. The triplet excitons also exhibited remarkably long diffusion length of 152 nm, ensuring their transport across the entire thin film.

4.2. Electron–Phonon Coupling and Polaron Formation

Electron–phonon coupling (EPC) refers to the interaction of charge carriers with lattice vibrations (phonons), which is critical to charge carrier recombination dynamics in perovskites. Phonon scattering of charges limits the carrier mobilities, modulates the cooling process of hot carriers and governs the broadening of emission line. Currently, the knowledge of EPC in 3D perovskites has been well-established based on both experimental and theoretic studies. The EPC in 2D perovskites is believed to be further regulated by the strong excitonic feature of the photogenerated species.

The EPC in atomically thin 2D perovskites was initially investigated by temperature dependent PL dynamics.[61] A power law dependence of observed scattering rate T^{γ} ($\gamma > 0$) indicated that phonons were the main sources of scattering because scattering by charge impurities would lead to an opposite trend over temperature. In principle, there exist three possible types of phonons that could account for the carrier scattering—i) acoustic phonon via deformation potential mechanism, ii) in-plane polar optical phonons through Frölich interaction, and iii) out-of-plane homopolar (i.e., nonpolar) phonons via deformation potential. **Figure 8**a shows the fitted exponent γ of 1.9 and 1.6 for interband and intraband recombination, respectively. This indicated that carriers in 2D perovskites were mainly scattered by acoustic phonon and homopolar optical phonons while the scattering from the charged defects and polar optical phonons would be suppressed.

The above observation suggested the formation of strongly coupled polarons. The interaction of charges and neighboring ionic lattice resulted in the lattice deformation and consequently self-trapped the interacted charges. The properties of polarons depended on phonon coupling, particularly with longitudinal optical phonons.[61] First-principle calculation on both ground-state and excited state structures further proved the formation of polarons in 2D hybrid perovskites $(EDBE)PbCl_4$ and $(EDBE)PbBr_4$.[67] Once one electron was removed from or added to the calculated cluster, an obvious Pb—Cl bond shortening or elongation can be obtained as shown in Figure 8b, thus remarkably deforming the local geometry of the cluster. The results pointed to the formation of polarons with a large E_b in the range of 0.4–1.2 eV.

On the other hand, the EPC in 2D perovskites can also be monitored by the temperature evolution of the PL linewidth.[61,68] In a typical $(PEA)_2PbI_4$ thin layer, the excitonic absorption and PL spectra exhibited splitted photonic side bands corresponding to various phonon resonance. The energy spacing between those side bands can be a fingerprint to identify the coupled phonon modes in 2D perovskites. It also uncovered the existence of coupling to phonons that were located in both the organic and inorganic components of 2D perovskites.[68] Further investigation found that the unconventional EPC to organic cations in 2D perovskites facilitated

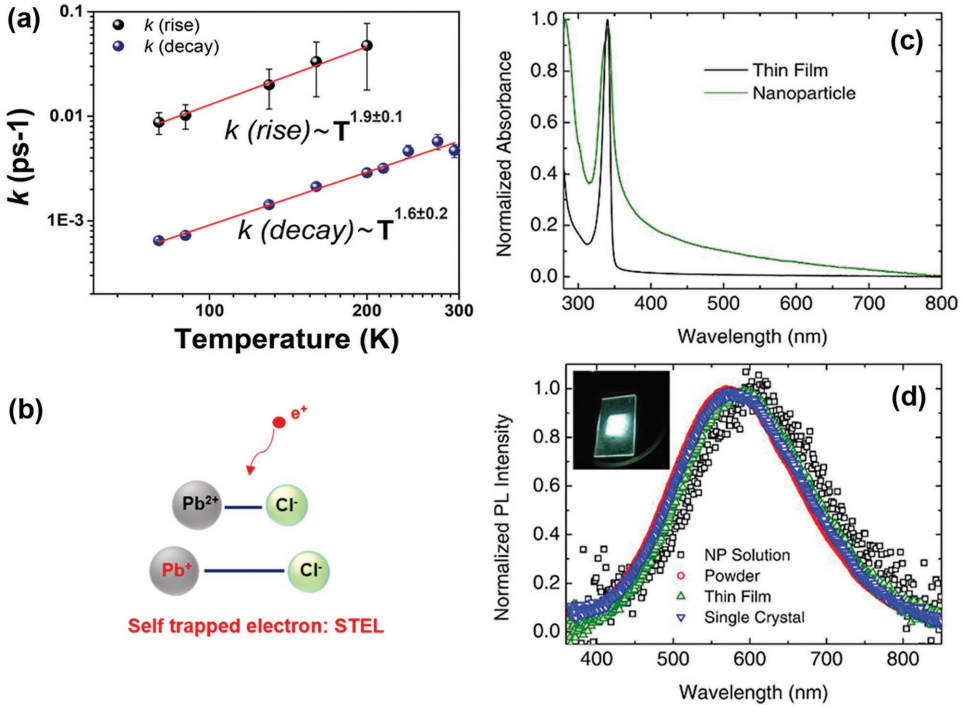

Figure 8. a) Power temperature-dependence of PL rise and decay rates in $(BA)_2PbI_4$ perovskite. b) Formation of self-trapped electrons from DFT calculation in $(EDBE)_{32}Pb_{12}Cl_{56}$ cluster. c) The absorption and d) PL spectra showing white-light emission of $(PEA)_2PbCl_4$. a) Reproduced with permission.[61] Copyright 2016, American Chemical Society. b) Reproduced with permission.[67] Copyright 2017, American Chemical Society. c,d) Reproduced with permission.[69] Copyright 2017, American Chemical Society.

the white-light emission in solution-processed $(PEA)_2PbCl_4$ perovskites at room temperature as shown in Figure 8c,d.[69] The $(PEA)_2PbCl_4$ exhibited a remarkably high color rendering index and photostability, making it ideal for natural white LED applications. This work suggests that the organic framework is not acting merely as an inert spacer and instead it is of critical importance to select an appropriate combination of the inorganic and organic components.

5. Conclusions and Outlook

In this article, we have reviewed recent advances in 2D Ruddlesden–Popper perovskites for optoelectronic applications. In order to achieve optimal devices, one critical concern in this type of perovskites is a delicate balance between hydrophobicity and charge conductivity. The hydrophobic organic spacers that improve the air-stability of 2D perovskites, however, undermine their electrical conductivity in thin film and hence constrain the charge transport in device. Therefore, structural optimization of the organic spacers is highly demanded for optoelectronics with a balance of efficiency and stability. It has been demonstrated that a variation of the length and linearity of the alkyl chain in the spacer molecules, an insertion of π-conjugated segment, and an incorporation of ammonium dications can enhance electronic coupling between the separated quantum wells in 2D perovskites. In particular, 2D perovskites with larger n values along with 2D/3D hybrids or heterojunctions result in lower bandgaps and higher carrier mobility while maintaining good ambient stability. However, the experimental results exhibit large complexity for designing of the above molecular structures and device architectures, which suffers from diversification of film morphologies, distortion of lattice structures and variation of electronic states. All of them would greatly influence the overall device performance. Under this circumstance, it is impossible to derive an explicit experimental trend from state-of-art research on materials engineering of 2D perovskites. Rather, the know-how should be established individually from case to case. To achieve that, investigation on fundamental photophysics is urgently needed in future studies including transportation mechanism of charge carriers, light coupling properties, and photo-induced dynamics of defect states, which is yet far less reported compared to those efforts on materials engineering.

On the other hand, the existence of local confinement as well as asymmetric dimensionality in 2D perovskites paves a way to modulate the optoelectronic properties. This involves internal charge redistribution of couple/decouple photogenerated charges to induce enhanced/inhibited recombination dynamics for solar cell applications, while engineering of the electron–phonon coupling enables to modify the line width of the PL emission toward white-light emission. Therefore, we anticipate the boarder applications of 2D perovskites as compared to their 3D counterparts.

Acknowledgements

This work was supported by Inter-Governmental International Cooperation Project of Science and Technology Commission of Shanghai Municipality (STCSM) under grant No. 17520710100 (Z.L.). K.Z. also acknowledges the support from Swedish Research Council, KAW foundation and NPRP grant #NPRP7-227-1-034 obtained from the Qatar National Research Fund (a member of Qatar Foundation).

Conflict of Interest

The authors declare no conflict of interest.

Keywords

2D perovskites, charge transport, molecular structures, optoelectronics, Ruddlesden–Popper

Received: June 22, 2017
Revised: July 24, 2017
Published online: October 13, 2017

[1] A. Kojima, K. Teshima, Y. Shirai, T. Miyasaka, *J. Am. Chem. Soc.* **2009**, *131*, 6050.
[2] J.-H. Im, C.-R. Lee, J.-W. Lee, S.-W. Park, N.-G. Park, *Nanoscale* **2011**, *3*, 4088.
[3] H.-S. Kim, C.-R. Lee, J.-H. Im, K.-B. Lee, T. Moehl, A. Marchioro, S.-J. Moon, R. Humphry-Baker, J.-H. Yum, J. E. Moser, M. Grätzel, N.-G. Park, *Sci. Rep.* **2012**, *2*, 591.
[4] M. M. Lee, J. Teuscher, T. Miyasaka, T. N. Murakami, H. J. Snaith, *Science* **2012**, *338*, 643.
[5] M. Liu, M. B. Johnston, H. J. Snaith, *Nature* **2013**, *501*, 395.
[6] J. Berry, T. Buonassisi, D. A. Egger, G. Hodes, L. Kronik, Y.-L. Loo, I. Lubomirsky, S. R. Marder, Y. Mastai, J. S. Miller, D. B. Mitzi, Y. Paz, A. M. Rappe, I. Riess, B. Rybtchinski, O. Stafsudd, V. Stevanovic, M. F. Toney, D. Zitoun, A. Kahn, D. Ginley, D. Cahen, *Adv. Mater.* **2015**, *27*, 5102.
[7] K. X. Steirer, P. Schulz, G. Teeter, V. Stevanovic, M. Yang, K. Zhu, J. J. Berry, *ACS Energy Lett.* **2016**, *1*, 360.
[8] Y. Rong, L. Liu, A. Mei, X. Li, H. Han, *Adv. Energy Mater.* **2015**, *5*, 1501066.
[9] Z. Wang, Z. Shi, T. Li, Y. Chen, W. Huang, *Angew. Chem. Int. Ed.* **2017**, *56*, 1190.
[10] S. N. Ruddlesden, P. Popper, *Acta Crystallogr.* **1957**, *10*, 538.
[11] S. N. Ruddlesden, P. Popper, *Acta Crystallogr.* **1958**, *11*, 54.
[12] D. H. Cao, C. C. Stoumpos, O. K. Farha, J. T. Hupp, M. G. Kanatzidis, *J. Am. Chem. Soc.* **2015**, *137*, 7843.
[13] I. C. Smith, E. T. Hoke, D. Solis-Ibarra, M. D. McGehee, H. I. Karunadasa, *Angew. Chem. Int. Ed.* **2014**, *53*, 11232.
[14] L. Pedesseau, D. Sapori, B. Traore, R. Robles, H.-H. Fang, M. A. Loi, H. Tsai, W. Nie, J.-C. Blancon, A. Neukirch, S. Tretiak, A. D. Mohite, C. Katan, J. Even, M. L. Kepenekian, *ACS Nano* **2016**, *10*, 9776.
[15] M. Yuan, L. N. Quan, R. Comin, G. Walters, R. Sabatini, O. Voznyy, S. Hoogland, Y. Zhao, E. M. Beauregard, P. Kanjanaboos, Z. Lu, D. H. Kim, E. H. Sargent, *Nat. Nanotechnol.* **2016**, *11*, 872.
[16] H. Tsai, W. Nie, J.-C. Blancon, C. C. Stoumpos, R. Asadpour, B. Harutyunyan, A. J. Neukirch, R. Verduzco, J. J. Crochet, S. Tretiak, L. Pedesseau, J. Even, M. A. Alam, G. Gupta, J. Lou, P. M. Ajayan, M. J. Bedzyk, M. G. Kanatzidis, A. D. Mohite, *Nature* **2016**, *536*, 312.
[17] Y. Chen, M. He, J. Peng, Y. Sun, Z. Liang, *Adv. Sci.* **2016**, *3*, 1500392.
[18] X. Hong, T. Ishihara, A. V. Nurmikko, *Phys. Rev. B* **1992**, *45*, 6961.
[19] M. E. Kamminga, H.-H. Fang, M. R. Filip, F. Giustino, J. Baas, G. R. Blake, M. A. Loi, T. T. M. Palstra, *Chem. Mater.* **2016**, *28*, 4554.
[20] J. Gebhardt, Y. Kim, A. M. Rappe, *J. Phys. Chem. C* **2017**, *121*, 6569.

[21] Y. Yang, D. P. Ostrowski, R. M. France, K. Zhu, J. van de Lagemaat, J. M. Luther, M. C., *Nat. Photonics* **2016**, *10*, 53.
[22] T. Ishihara, *J. Lumin.* **1994**, *60–61*, 269.
[23] W. Liu, J. Xing, J. Zhao, X. Wen, K. Wang, P. Lu, Q. Xiong, *Adv. Optical Mater.* **2017**, *5*, 1601045.
[24] D. Liang, Y. Peng, Y. Fu, M. J. Shearer, J. Zhang, J. Zhai, Y. Zhang, R. J. Hamers, T. L. Andrew, S. Jin, *ACS Nano* **2016**, *10*, 6897.
[25] T. Matsushima, S. Hwang, A. S. D. Sandanayaka, C. Qin, S. Terakawa, T. Fujihara, M. Yahiro, C. Adachi, *Adv. Mater.* **2016**, *28*, 10275.
[26] T. Matsushima, F. Mathevet, B. Heinrich, S. Terakawa, T. Fujihara, C. Qin, A. S. D. Sandanayaka, J.-C. Ribierre, C. Adachi, *Appl. Phys. Lett.* **2016**, *109*, 253301.
[27] Y. Liao, H. Liu, W. Zhou, D. Yang, Y. Shang, Z. Shi, B. Li, X. Jiang, L. Zhang, L. N. Quan, R. Quintero-Bermudez, B. R. Sutherland, Q. Mi, E. H. Sargent, Z. Ning, *J. Am. Chem. Soc.* **2017**, *139*, 6693.
[28] C. C. Stoumpos, D. H. Cao, D. J. Clark, J. Young, J. M. Rondinelli, J. I. Jang, J. T. Hupp, M. G. Kanatzidis, *Chem. Mater.* **2016**, *28*, 2852.
[29] D. Wang, B. Wen, Y.-N. Zhu, C.-J. Tong, Z.-K. Tang, L.-M. Liu, *J. Phys. Chem. Lett.* **2017**, *8*, 876.
[30] Y. Chen, Y. Sun, J. Peng, W. Zhang, X. Su, K. Zheng, T. Pullerits, Z. Liang, *Adv. Energy Mater.* **2017**, *7*, 1700162.
[31] D. H. Cao, C. C. Stoumpos, T. Yokoyama, J. L. Logsdon, T.-B. Song, O. K. Farha, M. R. Wasielewski, J. T. Hupp, M. G. Kanatzidis, *ACS Energy Lett.* **2017**, *2*, 982.
[32] Z. Tan, Y. Wu, H. Hong, J. Yin, J. Zhang, L. Lin, M. Wang, X. Sun, L. Sun, Y. Huang, K. Liu, Z. Liu, H. Peng, *J. Am. Chem. Soc.* **2016**, *138*, 16612.
[33] J. Zhou, Y. Chu, J. Huang, *ACS Appl. Mater. Interfaces* **2016**, *8*, 25660.
[34] L. Dou, A. B. Wong, Y. Yu, M. Lai, N. Kornienko, S. W. Eaton, A. Fu, C. G. Bischak, J. Ma, T. Ding, N. S. Ginsberg, L.-W. Wang, A. P. Alivisatos, P. Yang, *Science* **2015**, *349*, 1519.
[35] S. Nagane, S. Ogale, *J. Phys. Chem. Lett.* **2016**, *7*, 4757.
[36] H. Hu, T. Salim, B. Chen, Y. M. Lam, *Sci. Rep.* **2016**, *6*, 33546.
[37] Z. Xiao, R. A. Kerner, L. Zhao, N. L. Tran, K. Lee, T.-W. Koh, G. D. Scholes, B. P. Rand, *Nat. Photonics* **2017**, *11*, 108.
[38] Z. Yang, E. Yassitepe, O. Voznyy, A. Janmohamed, X. Lan, L. Levina, R. Comin, E. H. Sargent, *J. Am. Chem. Soc.* **2015**, *137*, 14869.
[39] J.-F. Liao, H.-S. Rao, B.-X. Chen, D.-B. Kuang, C.-Y. Su, *J. Mater. Chem. A* **2017**, *5*, 2066.
[40] L. Ma, J. Dai, X. C. Zeng, *Adv. Energy Mater.* **2017**, *7*, 1601731.
[41] R. Hamaguchi, M. Yoshizawa-Fujita, T. Miyasaka, H. Kunugita, K. Ema, Y. Takeoka, M. Rikukawa, *Chem. Commun.* **2017**, *53*, 4366.
[42] C. F. Ferreira, E. E. Pérez-Cordero, K. A. Abboud, D. R. Talham, *Chem. Mater.* **2016**, *28*, 5522.
[43] J. Cho, Y.-H. Choi, T. E. O'Loughlin, L. D. Jesus, S. Banerjee, *Chem. Mater.* **2016**, *28*, 6909.
[44] C. Lermer, S. T. Birkhold, I. L. Moudrakovski, P. Mayer, L. M. Schoop, L. Schmidt-Mende, B. V. Lotsch, *Chem. Mater.* **2016**, *28*, 6560.
[45] M. C. Weidman, M. Seitz, S. D. Stranks, W. A. Tisdale, *ACS Nano* **2016**, *10*, 7830.
[46] D. Yu, F. Cao, Y. Shen, X. Liu, Y. Zhu, H. Zeng, *J. Phys. Chem. Lett.* **2017**, *8*, 2565.
[47] Z. Chen, C. Zhang, X.-F. Jiang, M. Liu, R. Xia, T. Shi, D. Chen, Q. Xue, Y.-J. Zhao, S. Su, H.-L. Yip, Y. Cao, *Adv. Mater.* **2017**, *29*, 1603157.
[48] N. Wang, L. Cheng, R. Ge, S. Zhang, Y. Miao, W. Zou, C. Yi, Y. Sun, Y. Cao, R. Yang, Y. Wei, Q. Guo, Y. Ke, M. Yu, Y. Jin, Y. Liu, Q. Ding, D. Di, L. Yang, G. Xing, H. Tian, C. Jin, F. Gao, R. H. Friend, J. Wang, W. Huang, *Nat. Photonics* **2016**, *10*, 699.
[49] S. Zhang, C. Yi, N. Wang, Y. Sun, W. Zou, Y. Wei, Y. Cao, Y. Miao, R. Li, Y. Yin, N. Zhao, J. Wang, W. Huang, *Adv. Mater.* **2017**, *29*, 1606600.
[50] K. Jemli, P. Audebert, L. Galmiche, G. Trippe-Allard, D. Garrot, J.-S. Lauret, E. Deleporte, *ACS Appl. Mater. Interfaces* **2015**, *7*, 21763.
[51] L. Mao, Y. Wu, C. C. Stoumpos, M. R. Wasielewski, M. G. Kanatzidis, *J. Am. Chem. Soc.* **2017**, *139*, 5210.
[52] M. Safdari, P. H. Svensson, M. T. Hoang, I. Oh, L. Kloo, J. M. Gardner, *J. Mater. Chem. A* **2016**, *4*, 15638.
[53] T. Zhao, C.-C. Chueh, Q. Chen, A. Rajagopal, A. K.-Y. Jen, *ACS Energy Lett.* **2016**, *1*, 757.
[54] M. D. Birowosuto, D. Cortecchia, W. Drozdowski, K. Brylew, W. Lachmanski, A. Bruno, C. Soci, *Sci. Rep.* **2016**, *6*, 37254.
[55] T. Zhang, L. Xie, L. Chen, N. Guo, G. Li, Z. Tian, B. Mao, Y. Zhao, *Adv. Funct. Mater.* **2017**, *27*, 1603568.
[56] B.-E. Cohen, M. Wierzbowska, L. Etgar, *Adv. Funct. Mater.* **2017**, *27*, 1604733.
[57] J. Byun, H. Cho, C. Wolf, M. Jang, A. Sadhanala, R. H. Friend, H. Yang, T.-W. Lee, *Adv. Mater.* **2016**, *28*, 7515.
[58] N. Li, Z. Zhu, C.-C. Chueh, H. Liu, B. Peng, A. Petrone, X. Li, L. Wang, A. K.-Y. Jen, *Adv. Energy Mater.* **2017**, *7*, 1601307.
[59] Y. Hu, J. Schlipf, M. Wussler, M. L. Petrus, W. Jaegermann, T. Bein, P. Müller-Buschbaum, P. Docampo, *ACS Nano* **2016**, *10*, 5999.
[60] G. Grancini, C. Roldán-Carmona, I. Zimmermann, E. Mosconi, X. Lee, D. Martineau, S. Narbey, F. Oswald, F. D. Angelis, M. Graetzel, M. K. Nazeeruddin, *Nat. Commun.* **2017**, *8*, 15684.
[61] Z. Guo, X. Wu, T. Zhu, X. Zhu, L. Huang, *ACS Nano* **2016**, *10*, 9992.
[62] G. Xing, B. Wu, X. Wu, M. Li, B. Du, Q. Wei, J. Guo, E. K. L. Yeow, T. C. Sum, W. Huang, *Nat. Commun.* **2017**, *8*, 14558.
[63] R. L. Milot, R. J. Sutton, G. E. Eperon, A. A. Haghighirad, J. M. Hardigree, L. Miranda, H. J. Snaith, M. B. Johnston, L. M. Herz, *Nano Lett.* **2016**, *16*, 7001.
[64] J.-C. Blancon, H. Tsai, W. Nie, C. C. Stoumpos, L. Pedesseau, C. Katan, M. Kepenekian, C. M. M. Soe, K. Appavoo, M. Y. Sfeir, S. Tretiak, P. M. Ajayan, M. G. Kanatzidis, J. Even, J. J. Crochet, A. D. Mohite, *Science* **2017**, *355*, 1288.
[65] J. Liu, J. Leng, K. Wu, J. Zhang, S. Jin, *J. Am. Chem. Soc.* **2017**, *139*, 1432.
[66] R. Younts, H.-S. Duan, B. Gautam, B. Saparov, J. Liu, C. Mongin, F. N. Castellano, D. B. Mitzi, K. Gundogdu, *Adv. Mater.* **2017**, *29*, 1604278.
[67] J. Yin, H. Li, D. Cortecchia, C. Soci, J.-L. Brédas, *ACS Energy Lett.* **2017**, *2*, 417.
[68] D. B. Straus, S. H. Parra, N. Iotov, J. Gebhardt, A. M. Rappe, J. E. Subotnik, J. M. Kikkawa, C. R. Kagan, *J. Am. Chem. Soc.* **2016**, *138*, 13798.
[69] K. Thirumal, W. K. Chong, W. Xie, R. Ganguly, S. K. Muduli, M. Sherburne, M. Asta, S. Mhaisalkar, T. C. Sum, H. S. Soo, N. Mathews, *Chem. Mater.* **2017**, *29*, 3947.

